


RESEARCH ARTICLE

On the role of Ural Blocking in driving the Warm Arctic–Cold Siberia pattern

Evangelos Tyrlis¹  | Jürgen Bader^{1,2} | Elisa Manzini¹ | Jinro Ukita³ | Hisashi Nakamura⁴ | Daniela Matei¹¹Max Planck Institute for Meteorology, Hamburg, Germany²Uni Climate, Uni Research and the Bjerknes Centre for Climate Research, Bergen, Norway³Department of Environmental Sciences, Niigata University, Niigata, Japan⁴Research Center for Advanced Science and Technology, University of Tokyo, Tokyo, Japan**Correspondence**E. Tyrlis, Max Planck Institute for Meteorology, Hamburg, Germany.
Email: evangelos.tyrlis@mpimet.mpg.de**Funding information**

Max Planck Institute for Meteorology, Hamburg, Germany

Abstract

We use reanalysis data to substantiate the role of Ural blocking (UB) in driving the Warm Arctic–Cold Siberia (WACS) pattern, which represents an anti-correlation of surface temperature between the Barents–Kara Seas and central Asia. We confirm a robust link between UB and the WACS pattern on daily to subseasonal time-scales. UB controls the pace of the WACS pattern; warming over the Barents–Kara Seas and cooling over central Asia peak 3–5 days after the UB onset. The observed sea ice deficit over the Barents–Kara Seas in the weeks prior to UB onset is not statistically significant when the long-term trend in sea ice is removed. Thus, the sea ice deficit may not have a direct impact on UB occurrence but it develops as a delayed response to UB. The interannual variability of the WACS pattern is also strongly linked to UB. We identify an upward trend in wintertime UB in recent decades that accounts for a cooling rate of 1°C/decade over central Asia. Over the Barents–Kara Seas, UB trends explain a small fraction of the warming, which is dominated by Arctic amplification. Finally, the link between UB and the WACS pattern is statistically robust over the ERA-Interim period but weaker during the 1990s when the lowest UB activity was observed.

KEYWORDS

Arctic amplification, trends, Ural blocking, Warm Arctic–Cold Siberia pattern, winter

1 | INTRODUCTION

Arctic amplification has been associated with a weaker and increasingly meandering midlatitude westerly jet that favours blocking (Francis and Vavrus, 2012; 2015), and is related to more frequent weather extremes in midlatitudes.

An increase in cold spells over Eurasian and North American midlatitudes in recent decades has been reported (Zhang *et al.*, 2012; Cohen *et al.*, 2014; Horton *et al.*, 2015). However, the evidence for a recent increase in blocking activity across the Northern Hemisphere and a wavier jet has been disputed (Barnes, 2013; Barnes *et al.*, 2014).

This is an open access article under the terms of the Creative Commons Attribution-NonCommercial-NoDerivs License, which permits use and distribution in any medium, provided the original work is properly cited, the use is non-commercial and no modifications or adaptations are made.

© 2020 The Authors. *Quarterly Journal of the Royal Meteorological Society* published by John Wiley & Sons Ltd on behalf of the Royal Meteorological Society.

Overall, a heated debate (Fischer and Knutti, 2014; Barnes and Screen, 2015) exists between those studies that have provided evidence supporting a link between Arctic warming and midlatitude cooling (e.g., Mori *et al.*, 2014; Kug *et al.*, 2015; Ye *et al.*, 2018) and those that have failed to identify any significant connection (e.g., Screen *et al.*, 2013; Li *et al.*, 2015). A possible cause for this ongoing controversy is that, relative to observations, models appear to systematically underestimate Eurasian cooling in response to sea ice loss; almost half of the recently observed Eurasian cooling events can be attributed to sea ice loss (Mori *et al.*, 2019a). However, the precise method employed for the comparison of observational and modelling results can severely affect the interpretation of results (Mori *et al.*, 2019b; Screen and Blackport, 2019).

The maxima of warming and sea ice loss over the Barents–Kara Seas (BKS) emerging after the late 1990s have been associated with cooling in central Asian mid-latitudes (CAS): a link known as the Warm Arctic–Cold Siberia (WACS) or Warm Arctic–Cold Eurasia pattern (Mori *et al.*, 2014; 2019a). Given that the role of Ural blocking (UB) in inducing cold spells over central Asia is of paramount importance, the impact of BKS sea ice decline on UB activity has been extensively investigated in previous studies. During the period of rapid BKS warming after the year 2000, more persistent UB episodes occurred due to the weaker westerly flow over Eurasian mid-to-high latitudes (Luo *et al.*, 2016b), which resulted in even more enhanced BKS warming and midlatitude Eurasian cold anomalies (Yao *et al.*, 2017; Luo *et al.*, 2017c). Anomalous turbulent heat fluxes under BKS low sea ice conditions in late autumn were found to trigger a stationary Rossby wave train that can amplify the surface Siberian High and bring cold weather over east Asia (Honda *et al.*, 2009). A similar response was reported for a reduction of BKS sea ice by Petoukhov and Semenov (2010) and Orsolini *et al.* (2012). Inoue *et al.* (2012) reported that during years of low BKS sea ice, reduced storminess over the BKS occurs simultaneously with an anticyclonic anomaly around the Siberian coast and anomalous cold advection over Siberia, giving rise to the WACS pattern.

Recently, the meridional tropospheric potential vorticity (PV) gradient PV_y has been considered as a key physical mechanism that can explain the emergence of the WACS pattern. Luo *et al.* (2018, 2019b, 2019c) employed a nonlinear multiscale interaction model to show that the strength of PV_y is intrinsically linked to the nonlinearity and energy dispersion of blocking and ultimately its persistence. The weak climatological PV_y over Eurasian mid-to-high latitudes (weak PV barrier) favours more persistent UB. During the recent decades, PV_y has become even weaker over Eurasia due the intense warming and sea-ice loss over the BKS, leading to more persistent UB and contributing to

the increased cold winter trend in East Asia (Luo *et al.*, 2019b).

The link between Arctic climate change and midlatitude circulation anomalies through stratosphere–troposphere coupling has also been studied (Nakamura *et al.*, 2016; Sun *et al.*, 2016; Hoshi *et al.*, 2017). The BKS sea ice deficit or increased autumn snow cover over Siberia can enhance upward propagation of planetary wave activity, which can weaken the stratospheric polar vortex later in winter and induce a surface impact in the form of the WACS pattern over the BKS and Ural regions (Cohen *et al.*, 2014; Kretschmer *et al.*, 2016). In contrast, the observational analysis by Sorokina *et al.* (2016) and the modelling study by Peings (2019) provide evidence that does not support the argument that increased snowfall in Siberia and the sea ice deficit over the BKS in November can drive UB and the WACS pattern. Instead, the atmospheric circulation associated with UB can be seen as a key driver of sea ice anomalies over the Arctic. Also, UB episodes in November can enhance upward planetary wave activity, leading to early winter stratospheric warming followed by extreme weather events in midlatitudes during December and January (Peings, 2019; Tyrlis *et al.*, 2019).

Arctic sea ice retreat may favour UB occurrence, while the latter may have an amplifying effect on the WACS pattern and Arctic sea ice loss. Addressing causality is therefore not a trivial task; the feedback by UB cannot be disentangled with the use of seasonal averages because both processes act simultaneously. Recently, the role of UB as an amplifier of Arctic sea ice loss was investigated by Gong and Luo (2017) from a daily perspective. Sea ice decline over the BKS was found to be a delayed response to UB following its peak intensity by about 4 days. Chen *et al.* (2018) highlight the importance of quasi-stationary UB for inducing more efficient BKS sea ice loss at short time-scales.

The link between the Arctic and midlatitudes is also characterized by significant interdecadal variability. The strengthening of the teleconnection between the Arctic and midlatitudes in the late 1990s has been attributed to the stronger *midtropospheric warming* over the Arctic in recent decades (Xu *et al.*, 2019). In contrast, prior to the late 1990s, midlatitude atmospheric circulation anomalies over Eurasia barely correlate with Arctic *near-surface warming* because the latter lacks significant expansion to the midtroposphere. Intrinsic atmospheric dynamics are also important contributors to the recent cooling trends over central Eurasia and can augment influences through atmospheric teleconnections from remote sources, such as the tropical Pacific (e.g., Deser *et al.*, 2017). Anthropogenically induced Arctic warming is not necessarily the only driver of changes to the WACS pattern in recent decades;

internal atmospheric variability can also be significant. For example, Sung *et al.* (2018) provided evidence for a seemingly periodic interdecadal variation of the WACS pattern over the twentieth century that can be linked to internal atmospheric variability, specifically amplitude modulation of the climatological stationary waves over the North Atlantic on decadal time-scales.

Here we investigate the role of UB in driving the WACS pattern on short (synoptic to subseasonal) and interannual time-scales, as well as its trends. We employ a fully two-dimensional potential vorticity–potential temperature (PV– θ) blocking index to identify wintertime blocking episodes across the Northern Hemisphere (section 2). The PV– θ blocking index has not been used in previous studies and provides an alternative framework for studying the UB–WACS link. We regress blocking episode frequency on an objectively derived WACS index. Thus, without any a priori assumptions (e.g., averaging blocking frequency over a subjectively selected region), we can identify the regions where blocking induces temperature anomalies that markedly project onto the WACS pattern (section 3). We assess the robustness of the WACS pattern and the UB–WACS link over the ERA-Interim period (section 4). We then investigate the UB–WACS relation from a daily perspective to describe explicitly how the large-scale atmospheric circulation associated with UB drives the WACS pattern on short time-scales (section 5). Subsequently, we show that the interannual variability of the WACS pattern is strongly linked to UB, and we quantify the contribution of recent UB trends to the cooling trend over CAS (section 6). Finally, section 7 summarizes the results and presents conclusions.

2 | DATA AND METHODS

We diagnose the atmospheric circulation and state with variables from the ERA-Interim dataset (Dee *et al.*, 2011), which covers the period from January 1979 to June 2017. These include mean sea level pressure (MSLP), 2-m temperature (T2m), potential temperature (θ) on the 2-PVU (potential vorticity unit; $1 \text{ PVU} = 10^{-6} \text{ m}^2 \cdot \text{s}^{-1} \cdot \text{K} \cdot \text{kg}^{-1}$) surface, surface sensible heat flux (SSHF) and surface latent heat flux (SLHF). We also used data on sea ice cover (SIC) and sea surface temperature (SST) from the COBE dataset (Hirahara *et al.*, 2014), which covers the period from January 1979 to December 2016. Blocking is identified with the algorithm used in Tyrlis *et al.* (2015, 2019), which distinguishes blocking in areas of wave breaking, leading to reversals of the climatological meridional gradient of θ in the vicinity of the dynamical tropopause (see also Pelly and Hoskins, 2003). In the extratropical Northern Hemisphere, the dynamical tropopause is typically represented by the

2-PVU surface (e.g., Hoskins *et al.*, 1985). Following Berrisford *et al.* (2007) and Woollings *et al.* (2008), daily mean fields of θ on the 2-PVU surface are used to calculate the PV– θ blocking index on a 5° longitude by 4° latitude grid that extends over the latitudinal band $25\text{--}73^\circ\text{N}$. Local and instantaneous blocking is identified where the blocking index is positive. Large-scale blocking is identified where local and instantaneous blocking extends over a sector of at least 15° longitude. A *blocking event* is then defined at a specific longitude when large-scale blocking is identified within 10° longitude. A blocking event is referred to as a *blocking episode* (BE) if it lasts for 4 days or longer. The first day of a BE identified at a specific grid point is referred to as the BE onset day.

We calculate trends over the period 1991–2014, which is commonly used (e.g., Sun *et al.*, 2016) to capture the recent cooling with a pronounced WACS pattern. The statistical significance of the linear trends is evaluated using a two-sided t-test. A WACS index is defined in two ways: as the difference of area-averaged DJF-mean T2m over BKS minus that over CAS (hereafter WACSI), and as the second principal component (PC2). We apply an empirical orthogonal function (EOF) analysis to the non-detrended DJF mean T2m anomalies (1979–2017) over the domain ($0\text{--}180^\circ\text{E}$, $20\text{--}90^\circ\text{N}$). EOF analysis is also applied to the detrended DJF mean T2m anomalies and to subperiods of the ERA-Interim period to check the robustness of the WACS pattern and the UB–WACS link. The statistical significance of the area-averaged anomalies presented in Figures 8 and 9 is assessed with a Monte Carlo method. The same number of wintertime “BE onset days” is randomly sampled during the period 1979–2017, and the profiles illustrating the temporal evolution of the area-averaged anomalies are then reproduced. This process is repeated 100 times. For each day prior to/after the blocking onset, a distribution of artificially constructed anomalies is expected to capture the expected variability for this day. Finally, a UB day is identified as a *day of UB occurrence* when a BE is detected *anywhere* within the sector ($40\text{--}100^\circ\text{E}$, 61°N), referred to hereafter as the Ural sector.

3 | UB AND THE WACS PATTERN

The near-surface warming over the BKS exceeded 4°C per decade, while cooling is observed over CAS during 1991–2014 (Figure 1). Specifically, the regional cooling trend of 1.6°C per decade over CAS is attributed to the frequent occurrence of very cold winters during 2005–2014 (Figure 2). The dipole-like pattern of temperature trends over Eurasia and the Arctic, as a manifestation of the WACS pattern, coincided with an anticyclonic tendency

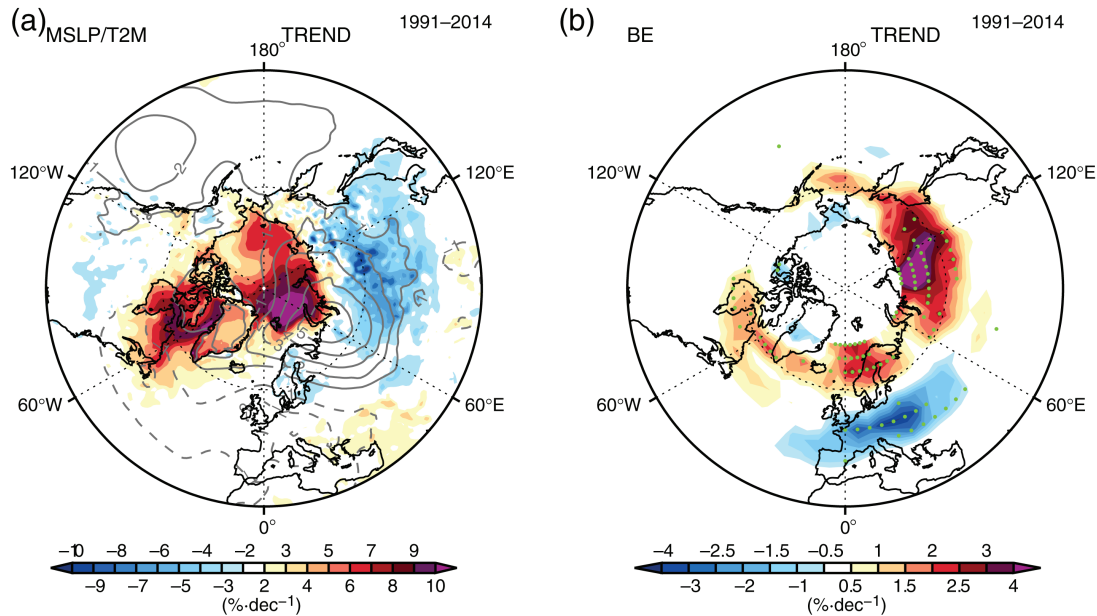


FIGURE 1 Linear trend of (a) December–February (DJF) mean sea level pressure (MSLP) (contours), 2-m temperature (T2M) (shaded areas) and (b) DJF mean blocking episode (BE) frequency (% per decade) during the period 1991–2014. The green dots in (b) mark the grid points where trends are statistically significant at the 95% level

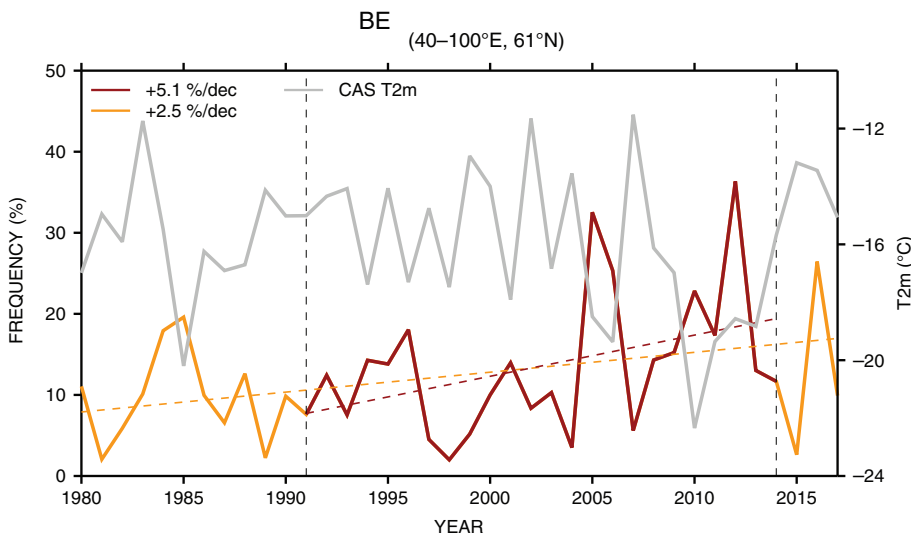


FIGURE 2 Evolution of area-averaged DJF mean T2m over CAS (60–100°E, 50–60°N; grey line) and BE frequency (Ural blocking episode [UBE] frequency; orange line) over the region 40–100°E, 61°N during the period 1979–2017; the period 1991–2014 is shown in red. The linear fit (dashed lines) is also illustrated and its slope is shown in the legend

to the south of the BKS (Figure 1a). Both the MSLP and T2m trends are statistically significant at the 95% confidence level during 1991–2014, though weaker over the whole ERA-Interim period (Figure S1). The anticyclonic tendency over the Ural region is related to an upward trend of blocking activity over subpolar Eurasia that exceeds 10% per decade to the southeast of the BKS (Figure 1b). The trend of the DJF mean BE frequency averaged over the Ural sector (i.e., Ural blocking episode, hereafter UBE; Figure 2) is statistically significant at the 95% confidence level and reaches +5.1% (+2.5%) per decade during the period 1991–2014 (1979–2017).

An upward trend in blocking activity around the Ural Mountains (60–100°E) was also reported by Luo *et al.* (2019b) during 1979–2013. However, unlike the positive trend of blocking activity found to the east of 100°E (Figure 2b), they identified a negative trend in blocking activity over the far east of Asia (their Figure 2). Such a discrepancy can be attributed to the different periods examined and the algorithms employed by the two studies for the identification of blocking. The investigation of case studies by Tyrlis *et al.* (2019) showed that the PV- θ blocking index can be more sensitive in identifying blocking episodes over Eurasia compared to the algorithms used by

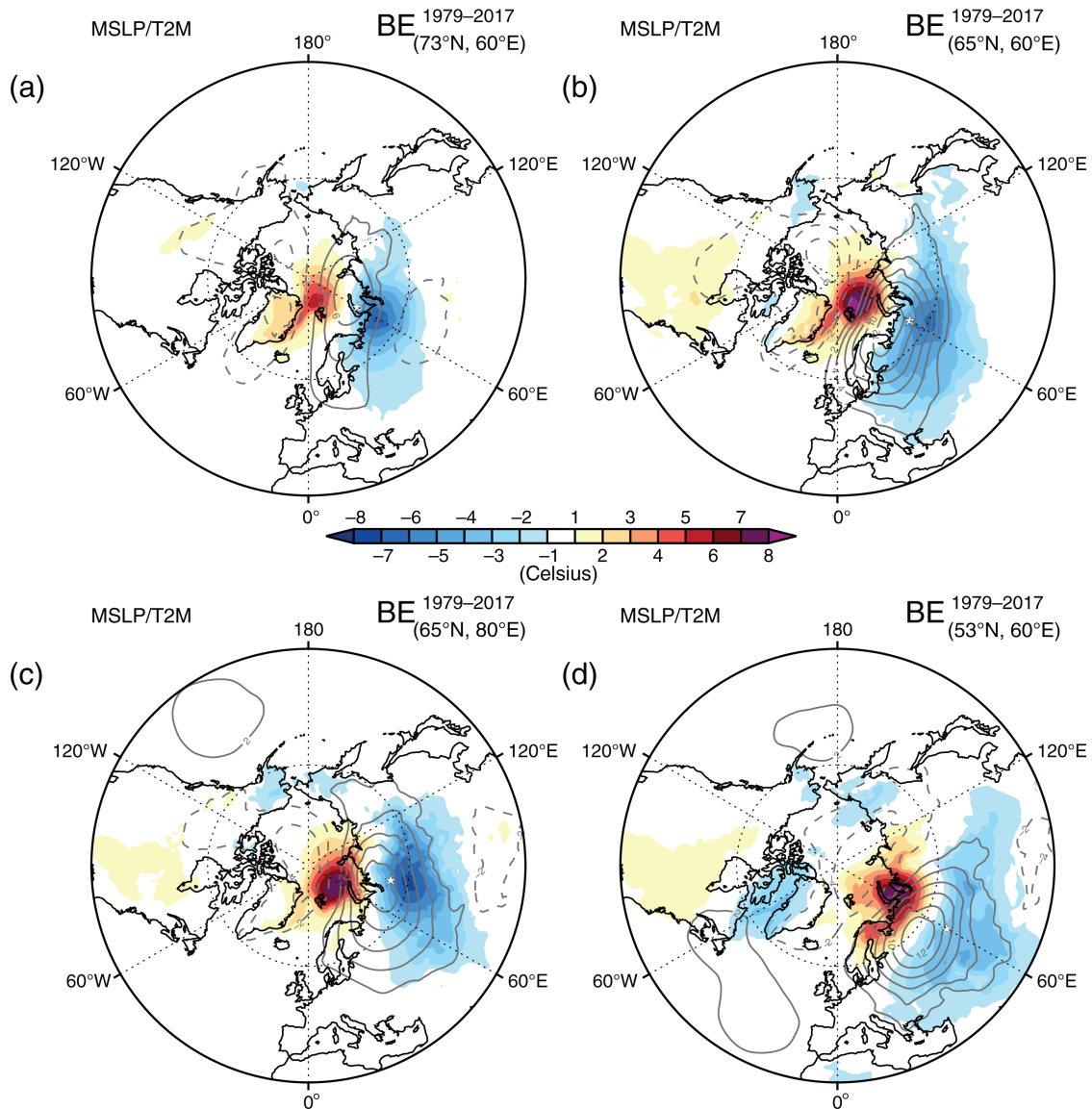


FIGURE 3 Composite mean departures of MSLP (contours) and T2M (shaded areas) from the climatological daily seasonal cycle for DJF days (1979–2017) when a BE is identified at (a) 60°E, 73°N; (b) 60°E, 65°N; (c) 80°E, 65°N and (d) 60°E, 53°N, as indicated by the stars

Chen *et al.* (2018) and Luo *et al.* (2019b), which are based on variants of the algorithms developed by Tibaldi and Molteni (1990) and Davini *et al.* (2012). Our results also agree with Luo *et al.* (2016b) who showed that blocking frequency was higher over the northern parts of the Ural region during the most recent part of the ERA-Interim period. Finally, although Barnes *et al.* (2014) found no clear hemispheric increase in winter blocking events over recent decades, central Asia (60–120°E) stands out as an exception for which a robust upward trend is identified (their Figure 3b).

Blocking induces a dipole of T2m anomalies with positive (negative) anomalies arising from warm (cold) advection to the north (south) of the blocking ridge (Figures 3 and S2). Regression of the hemisphere-wide

BE frequency on UBE frequency gives a homogeneous pattern throughout the Ural sector (Figure S3). Thus, any composites for blocking identified within the Ural sector, including those for 60°E as shown in Figure 3b, can be regarded as representative of UB. Nevertheless, BEs occurring to the east (60–90°E) of the Ural Mountains and at 60–65°N (Figure 3b,c) are particularly efficient at inducing a spatial pattern of cooling (warming) over CAS (BKS) that projects well onto the WACS pattern. The latitudinal position of blocking is also relevant; blocking off the Siberian coast can even induce cooling over parts of the BKS (Figure 3a), whereas midlatitude blocking can be related to warming over parts of Siberia (Figure 3d). Southward- and eastward-displaced UB events are particularly efficient at inducing persistent cold spells that can

affect South China under the positive phase of the North Atlantic Oscillation (NAO) (Luo *et al.*, 2016a). In conclusion, an increase in BE frequency is observed where the temperature dipole induced by blocking overwhelmingly projects onto the WACS pattern. Furthermore, the decreasing BE frequency after 2014 coincides with winters in which the cooling trend over CAS vanished (Figure 2).

To further substantiate the relation between UB and the WACS pattern, we follow Mori *et al.* (2014) to apply EOF analysis on the non-detrended DJF mean T2m anomalies (1979–2017) over the domain 0–180°E, 20–90°N. The first (second) EOF explains 29% (22%) of the total variance (Figure S4). The regressed fields of DJF mean T2m and MSLP anomalies on the first and second normalized principal components (PC1 and PC2) can be seen in Figure 4a,b, and the time series of PC1 and PC2 are depicted in Figure 4c,d (grey lines). EOF1 is associated with low-pressure anomalies along the Siberian coast, strong westerlies and warming over northern Eurasia. It is highly projected onto the Arctic Oscillation (AO): the correlation between PC1 and the AO index exceeds 0.85 (Mori *et al.*, 2014). EOF2 is characterized by anticyclonic circulation anomalies over the Ural Mountains and around the Siberian coast, as well as a dipole-like pattern of temperature anomalies featuring warming over the Arctic region and cooling over CAS. In fact, the statistically significant correlation between the WACSI and PC2 time series is 0.9 (Figure 4d). Thus, PC2 time series can be used as a proxy of the WACSI. Those winters belonging to the upper (lower) quartile of the PC1 and PC2 time series are marked with red (blue) dots in Figure 4c,d. Evidently, after the year 2000 an upward trend of the WACSI/PC2 can be identified and the overwhelming majority of high-WACSI/PC2 winters occurred after the year 2005, reflecting the more frequent occurrence of colder (warmer) winters in CAS (BKS). In contrast, extreme high and low PC1 values are evenly distributed throughout the ERA-Interim period.

Regression fields of BE frequency on PC1 and PC2, which are essentially the AO-like and WACS-pattern indices, respectively, are illustrated in Figure 4e,f. Alternatively, composite anomalies of BE frequency for winters belonging to the upper and lower PC quartiles are also provided (Figure S5). The negative (positive) phase of the AO-like mode coincides with frequent (rare) high-latitude blocking over the Ural sector north of 65°N. On the other hand, blocking occurring south of 65°N (defined in the sector 40–100°E as UB) emerges as the key phenomenon related to the WACS pattern. The maximum of the regression pattern is found for blocking within the domain (55–65°N, 70–90°E) (Figure 4f). Thus, the correlations between the PC2 and WACSI time series and that of the DJF mean BE frequency averaged over the longitudinal sector 40–100°E are higher for the sector centred at 61°N;

they are statistically significant and reach 0.73 and 0.84, respectively. Correlations are lower for sectors centred at higher latitudes (Figure S6). Higher-latitude blocking induces dipolar temperature anomalies that are shifted northwards as compared to the WACS pattern (Figure 3a). Both the interannual variability of the WACS intensity and its trend agree well with those of UB activity. In agreement with the analysis by Luo *et al.* (2016b), almost every peak in the WACSI/PC2 occurs in association with high UB activity. Subtle differences can be attributed to the use of different algorithms for identifying blocking. After the year 2000, the upward trend in the WACS intensity coincides with the positive trend of UB occurrence (Figure 4d).

4 | ROBUSTNESS OF THE WACS PATTERN AND THE UB-WACS LINK

The spatial WACS pattern does not change significantly over the ERA-Interim period. Application of EOF analysis to DJF mean T2m time series for two subperiods of equal length reveals that for both epochs the first two EOFs are very similar to their counterparts for the whole ERA-Interim period (Figure 5). The WACS pattern emerges as the second EOF and strong loadings are always found over the BKS and CAS. When the analysis is applied to detrended time series, for either epoch and for the overall ERA-Interim period, the WACS pattern once again emerges as the second EOF, retaining its dipolar character (Figure S7). Detrending causes weakening of the loading over the BKS, especially during the second epoch when the warming trend is stronger, and consequently the WACS pattern forms from two equally contributing nodes. In conclusion, WACS is a robust pattern that arises from true anti-correlation in T2m between the BKS and CAS but not from simultaneous occurrence, by chance, of opposite and perhaps unrelated T2m trends over these regions.

The UB-WACS link remains statistically significant throughout the ERA-Interim period but it is weaker during the 1990s (green line in Figure 6a). Using PC2 in place of WACSI, the correlation between UBE and PC2 is not statistically significant during that decade (green line in Figure 6b). The very low correlation between UB and PC1 suggests that the annular-like mode of variability over the Arctic is less strongly linked to lower-latitude UB. During the 1990s, when the lowest UBE activity is observed, other teleconnection patterns such as the AO or NAO might have increased their contributions to shaping the DJF mean T2m anomalies over the BKS and CAS. In addition to the reduced UBE frequency in the 1990s, changes in the UB-WACS link could be due to multidecadal modulations that can render the impact of UB on the CAS

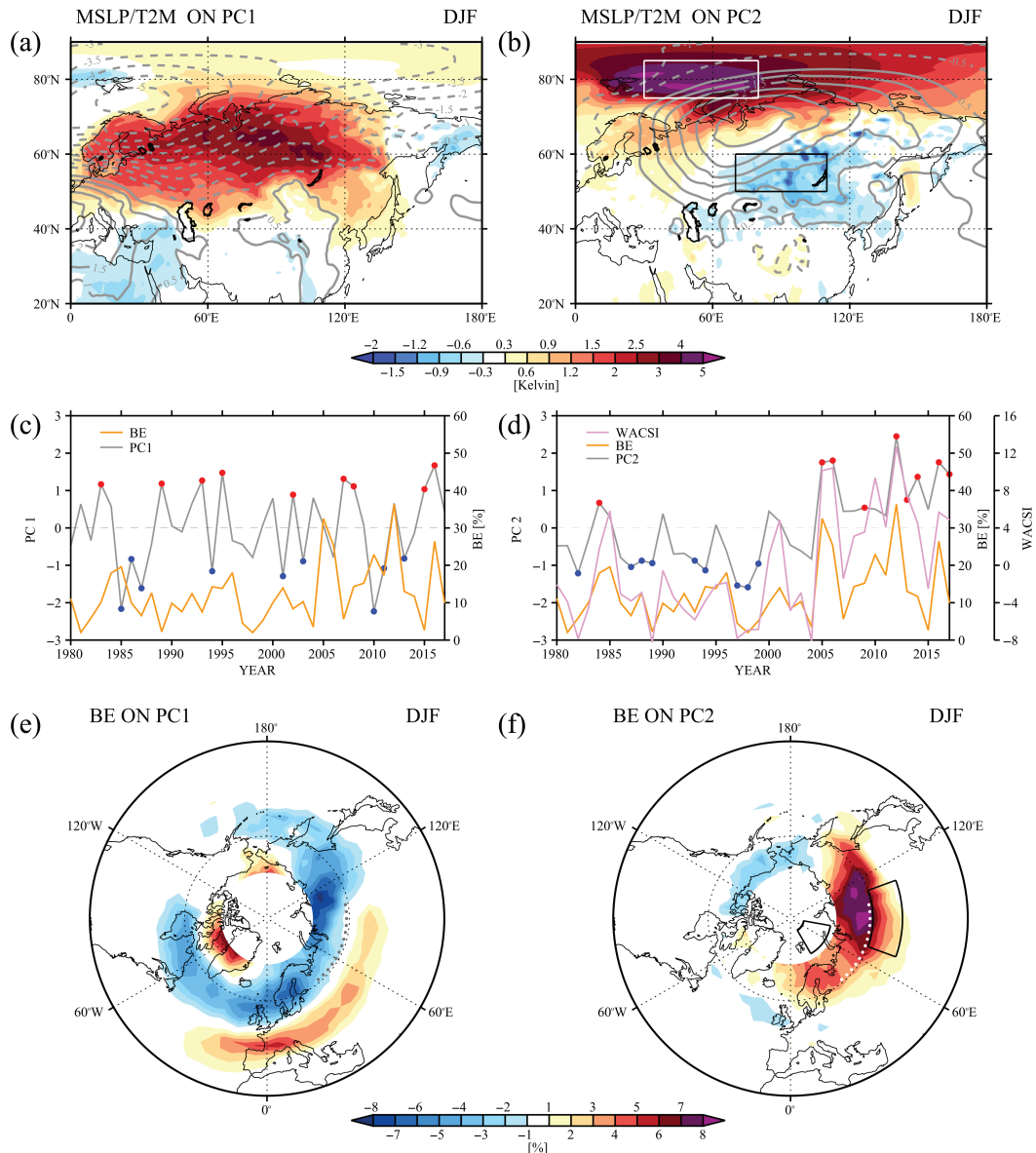


FIGURE 4 (a,b) Regression of DJF mean MSLP (contours) and T2M (shaded areas) on the normalized first (PC1) and second (PC2) principal components, respectively. (c,d) Interannual evolution of normalized PC1 and PC2 (grey lines), DJF mean blocking frequency (orange lines) averaged over the sector 40–100°E, 61°N (delineated by dots in e,f) and the WACS index (WACSI; purple line). Red (blue) dots mark winters belonging to the upper (lower) quartile of PC1 or PC2. (e,f) Regression of DJF mean blocking frequency on the normalized PC1 and PC2, respectively

non-stationary (e.g., Wang *et al.*, 2009; Wang and Chen, 2014). Cheung and Zhou (2015) investigated the daily to multidecadal impacts of UB on the Siberian High and T2m anomalies over the CAS and reported that the impacts are stronger when the North Atlantic jet stream is strongest and extends towards Eurasia. In conclusion, UB is indeed a key driver of the WACS pattern, driving T2m variability over *both* the BKS and CAS (Figure 6b). During the 1990s, the absence of UB resulted in a weakening of the correlations between UB and T2m over BKS/CAS, which were then re-established after the year 2000 when UB became frequent again. In agreement with our results, Xu *et al.*

(2019) also reported a strengthened midlatitude–Arctic linkage after the late 1990s. This may be associated with a deeper warming over the Arctic that extends to the midtroposphere and could trigger a stronger link between the Arctic and the midlatitudes.

The year-on-year variability of the DJF mean T2m has in recent years increased substantially over the Ural sector (Figure 7). Also, the explained variance of EOF2 (WACS) increased from 15% to 21% from the first epoch to the second, while the contribution from EOF1 has decreased. Therefore, the recent increase in the T2m variability is attributable to the emergence of the WACS pattern. The

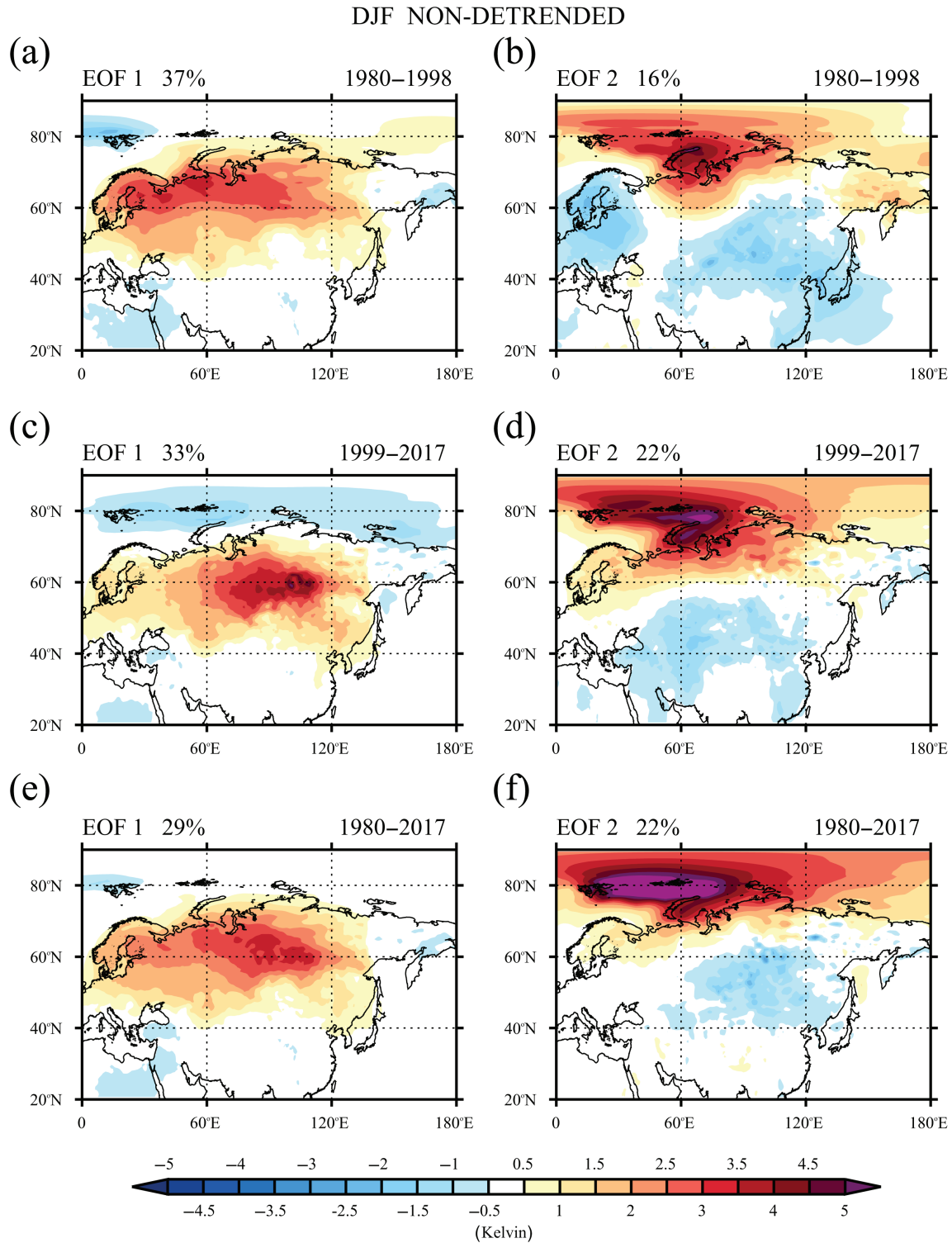
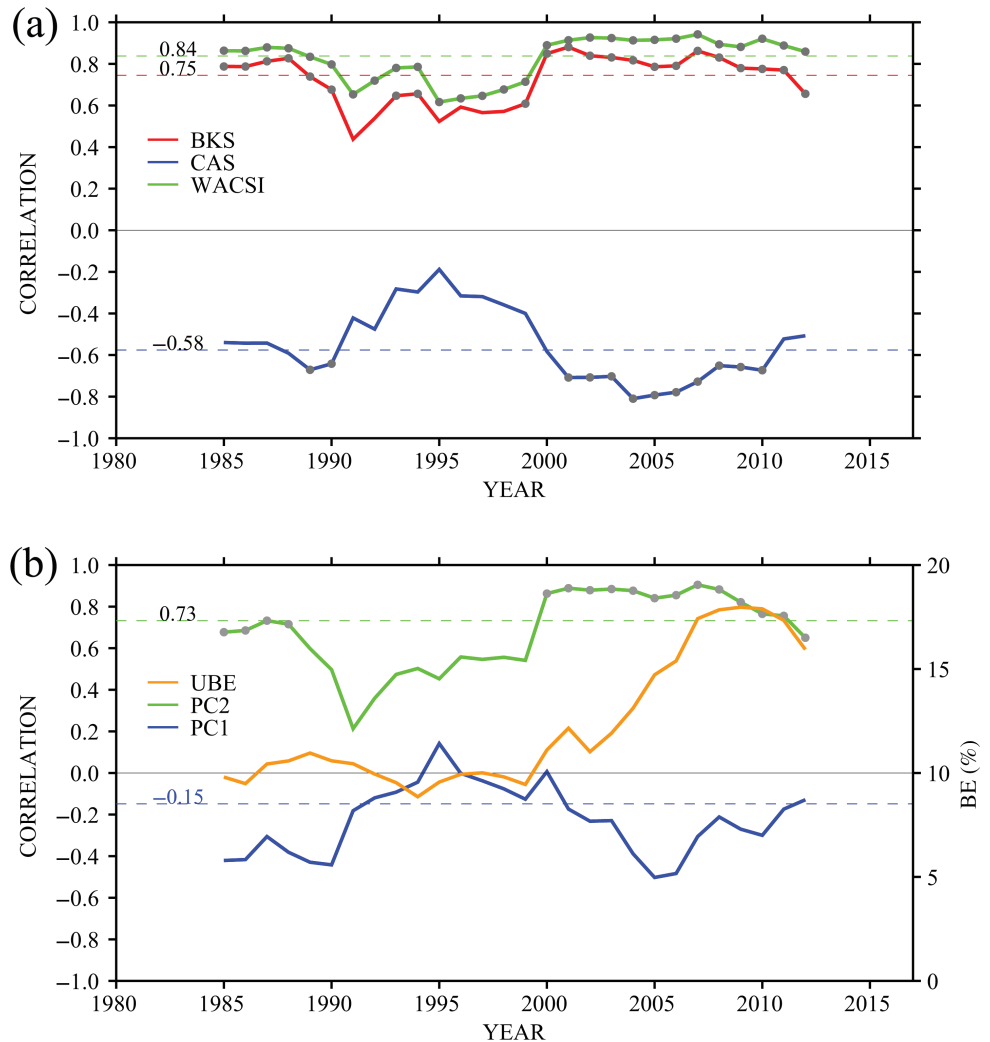


FIGURE 5 The left column (a,c,e) shows the first empirical orthogonal function (EOF), or EOF1, and the right column (b,d,f) shows the second EOF, or EOF2, resulting from EOF analysis applied on the non-detrended DJF mean T2m anomalies for (a,b) the first epoch (1980–1998), (c,d) the second epoch (1999–2017) and (e,f) the whole ERA-Interim period (1980–2017). EOF analysis is applied for T2m over the domain 0–180°E, 20–90°N

T2m variability increase is enhanced over the BKS and CAS, the two “centres of action” of the WACS pattern, and can thus be directly linked to the positive trend in UB activity. When the detrended T2m time series are used, the

dipolar pattern is still dominant. Nevertheless, only part of the variance is trend-related, especially over the Arctic. Undoubtedly, UB is key in driving the year-on-year T2m fluctuations over central Asia.

FIGURE 6 (a) Evolution of the correlation of DJF mean UBE with WACSI (green line), T2m-averaged over the BKS (red line) and CAS (blue line). Grey dots mark winters when the correlation is statistically significant at the 95% level. (b) Evolution of the correlation of DJF mean UBE frequency with PC1 (blue line) and PC2 (green line). The correlation is calculated for running 11-year windows. The orange line shows the UBE frequency (in %) averaged over the corresponding running windows. Horizontal dashed lines show the corresponding correlation but for the whole ERA-Interim period. The correlation is given in black bold type when it is found to be statistically significant at the 95% level



5 | UB DRIVING THE WACS PATTERN ON SHORT TIME-SCALES

Having identified that blocking within the domain 40–100°E, 60–65°N is closely related to the WACS pattern, we seek to elucidate the role of UB as a driving mechanism for the WACS pattern on shorter time-scales. All winter BE onset days are first identified at each grid point during 1979–2017 in order to construct composite anomalies for selected variables prior to and after the onset days. We show results corresponding to BE onset at 60°E, 61°N, but the results are similar for neighbouring grid points representing UB. The day-to-day evolution of area-averaged T2m over the BKS and CAS (Figure 8a,b), SST and SIC over the BKS (Figure 8f,g), and SSHF and SLHF over the BKS (Figure 8k,l) are depicted. Also, the evolution of composite anomalies of T2m/MSLP over Eurasia (Figure 8c–e) and SIC/SST (Figure 8h–j), as well as SSHF/SLHF (Figure 8m–o) over the Arctic, are illustrated for the periods –10 to –6 days, 0 to 4 days and 5 to 9 days relative to the blocking onset day. These

periods correspond to precursory conditions for UB, blocking development and decay, respectively.

Both the warming tendency over the BKS and the cooling tendency over CAS emerge out of the noise level synchronously with the UB onset, then build up quickly before peaking within 3–5 days *after* the onset day. This rapid evolution is due to the development of a strong anticyclonic circulation to the south of the BKS. The associated strong anomalous southwesterlies advect warm near-surface air towards the BKS, while cold north-northeasterly flow results in cold surges over CAS that can lead to subseasonal amplification of the cold Siberian High (Takaya and Nakamura, 2005). The thermal anomalies over the BKS and CAS persist for about 10 days, which is slightly higher than the mean duration (7–8 days) of winter UB (Tyrlis and Hoskins, 2008). Concurrently, an increase in SST and growth of the SIC deficit are observed. Note that SIC and SST were averaged over a rectangular domain (Figure 8j) that lies to the southwest of the one used to define the BKS T2m (Figure 8e). During winter the northern portion of the BKS is mostly covered with ice,

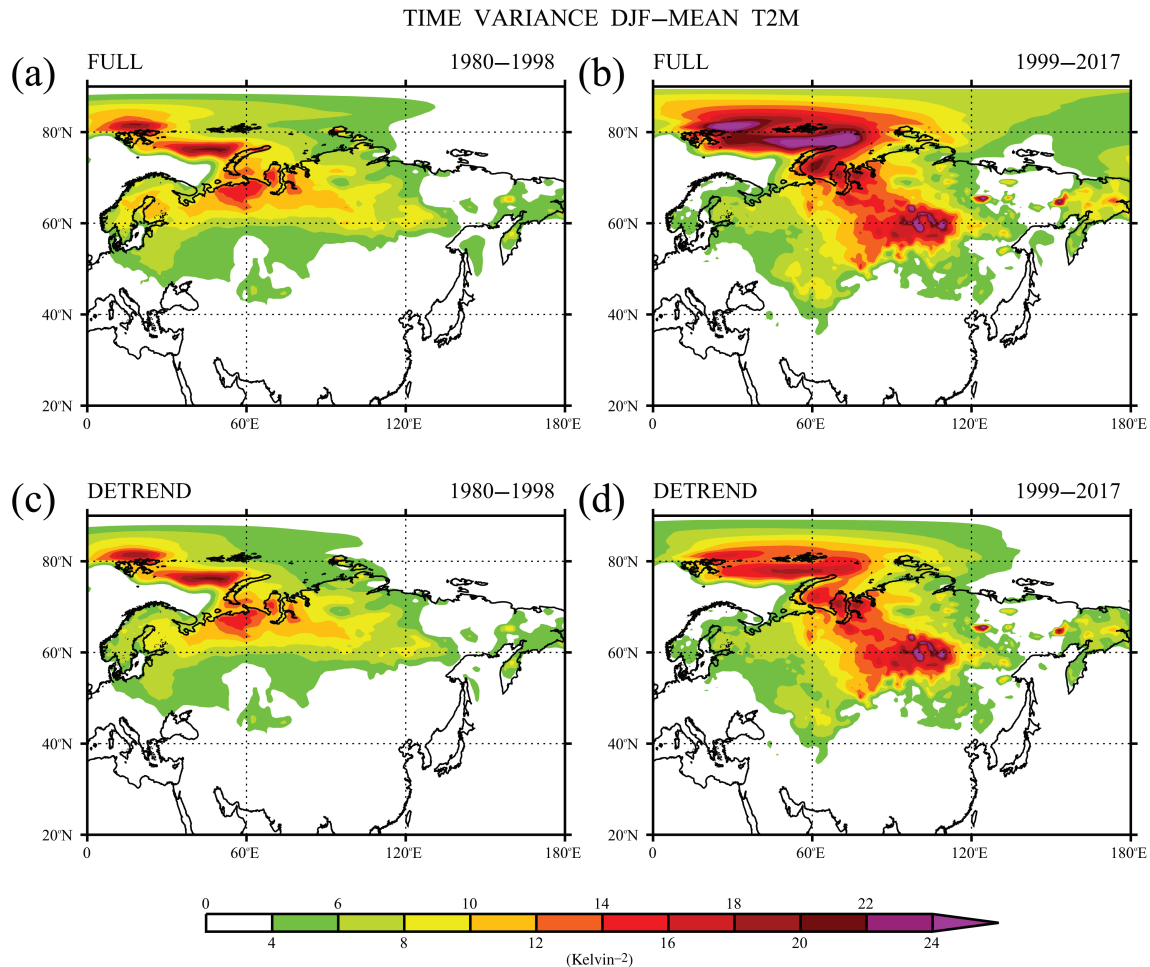


FIGURE 7 (a,b) Time variance (in K^2) of non-detrended time series of DJF mean T2m during (a) the first epoch (1980–1998) and (b) the second epoch (1999–2017) of the ERA-Interim period. (c,d) Time variance of detrended time series of the DJF mean T2m during (c) the first epoch and (d) the second epoch

while the largest variability in SIC/SST is observed in the southwestern portion. Compared with UB, both the SIC and SST anomalies develop more slowly and thus peak several days after the BE onset, while persisting for up to 20 days (Figure 8f–j).

The result is that the enhancement and decay of the sea ice deficit over the BKS is a slow process, which is in agreement with the daily assessment by Gong and Luo (2017). Here, we also examine the evolution of SIC and SST anomalies prior to the UB onset. UB emerges out of a background state that is biased towards positive SST and negative SIC anomalies of marginal significance (Figure 8f,g). However, as more UB onset days occurred near the end of the ERA-Interim period, composites are biased towards warm anomalies and the sea ice deficit over the BKS, both of which are related to Arctic amplification. Removal of the linear trends in the T2m, SST, SIC, SSHF and SLHF data results in the weakening of the positive SST and T2m anomalies, which are no longer statistically significant, in the period prior to the UB onset (Figure 9). This points to

an indication that the sea ice deficit in the weeks prior to the UB onset can be attributed to the presence of long-term trends in both sea ice and UB. Therefore, the sea ice deficit may not have a direct influence on UB occurrence. Such a result does not necessarily contradict other observational studies suggesting that winters with intense warming and sea ice decline over the BKS are accompanied by more persistent UB episodes (e.g., Luo *et al.*, 2018). Previous studies have investigated causality between BKS warming and the UB based on the analysis of winter means. However, UB can produce a feedback effect on BKS warming which can complicate addressing causality. The careful investigation of the composited signatures of the SST and SIC anomalies prior to the UB onset shown in Figure 9 may be more informative. Still, the impact of UB on enhancing the warming and sea ice deficit over the BKS is only slightly reduced after removing the background sea ice trend. Its temporal behaviour is unaffected and thus it remains a statistically robust result. The amplifying effect of the UB-induced circulation anomalies on the BKS sea ice loss is potentially

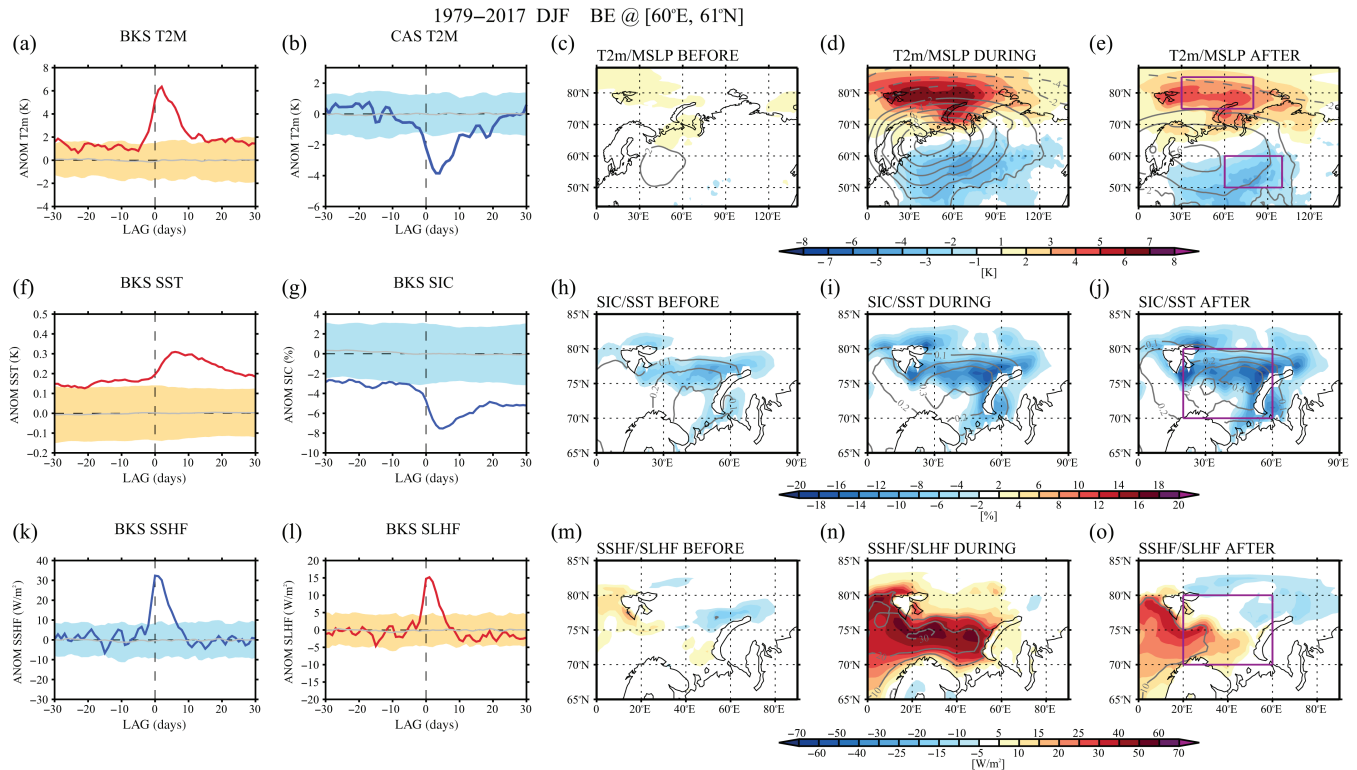


FIGURE 8 (a–e) Evolution of time mean MSLP (shaded areas) and T2m (contours) anomalies for the periods –10 to –6 days (c), 0 to 4 days (d) and 5 to 9 days (e) corresponding to phases relative to the DJF onset days (1979–2017) of UB at 60°E, 61°N. The day-to-day evolution of T2M averaged over the BKS (30–80°E, 75–85°N) and CAS (60–100°E, 50–60°N) is shown in (a) and (b), respectively. (f–j) As for (a–e) but for sea ice cover (SIC; shaded areas) and sea surface temperature (SST; contours). (k–o) As for (f–j) but for the surface sensible heat flux (SSHF; shaded areas) and the surface latent heat flux (SLHF; contours). SIC, SST, SSHF and SLHF are averaged over the region 20–60°E, 70°–80°N (boxes in j,o). Downward fluxes are positive (red shading). Shading delineates variability within two standard deviations; the thick grey line represents the mean of the distribution. Anomalies that lie outside the shading in the first two columns can be considered as statistically significant at the 95% level. The 95% confidence level was also constructed directly based on the 2.5th and 97.5th percentiles, and the assumption of Gaussianity was found to be valid

linked to the enhanced poleward intrusion of warm and moist air towards the BKS that occurs on the western side of the UB anticyclone, leading to the local intensification of downward infrared radiation (Woods and Caballero, 2013; Woods *et al.*, 2013; Gong and Luo, 2017; Lee *et al.*, 2017; Luo *et al.*, 2017a; Chen *et al.*, 2018).

Weak anomalous upward surface heat fluxes are observed prior to the UB onset (Figure 8k,l) in the vicinity of the weak positive SST anomalies and SIC deficit where upward heat transfer is favoured (Figure 8h). However, these anomalies are not statistically significant (Figure 8k,l) and their effect on the atmosphere could be negligible. Then, anomalous downward surface heat fluxes with high statistical significance develop with the surface anticyclonic anomaly associated with the UB. The anomalous warm advection over the BKS results in the reduction of the climatological upward surface heat fluxes. As the UB-associated anticyclonic anomaly matures and then decays, the anomalous downward fluxes (Figure 8n) gradually fade out and then weak anomalous upward fluxes

emerge, particularly over the northern and eastern portions of the domain where ice-free sea surface appears to expand (Figure 8j,o). Although the negative SIC anomaly diminishes slowly by around 20 days after the UB onset, the decay of the heat flux anomalies follows the faster weakening of the positive T2m anomaly. Thus, on daily to subseasonal time-scales, the anomalous surface fluxes are mainly driven by the atmospheric circulation anomalies associated with UB.

6 | THE UB INFLUENCE ON THE TEMPERATURE TRENDS OVER THE BKS AND CAS

To investigate the effect of UB on surface temperature separately over the BKS and CAS, the time series of the DJF mean T2m (T_{ALL}) is compared in Figure 10 to time series constructed for seasonal averages including UB days (BKS/CAS T_{BE}) and excluding UB days (BKS/CAS T_{NOBE}).

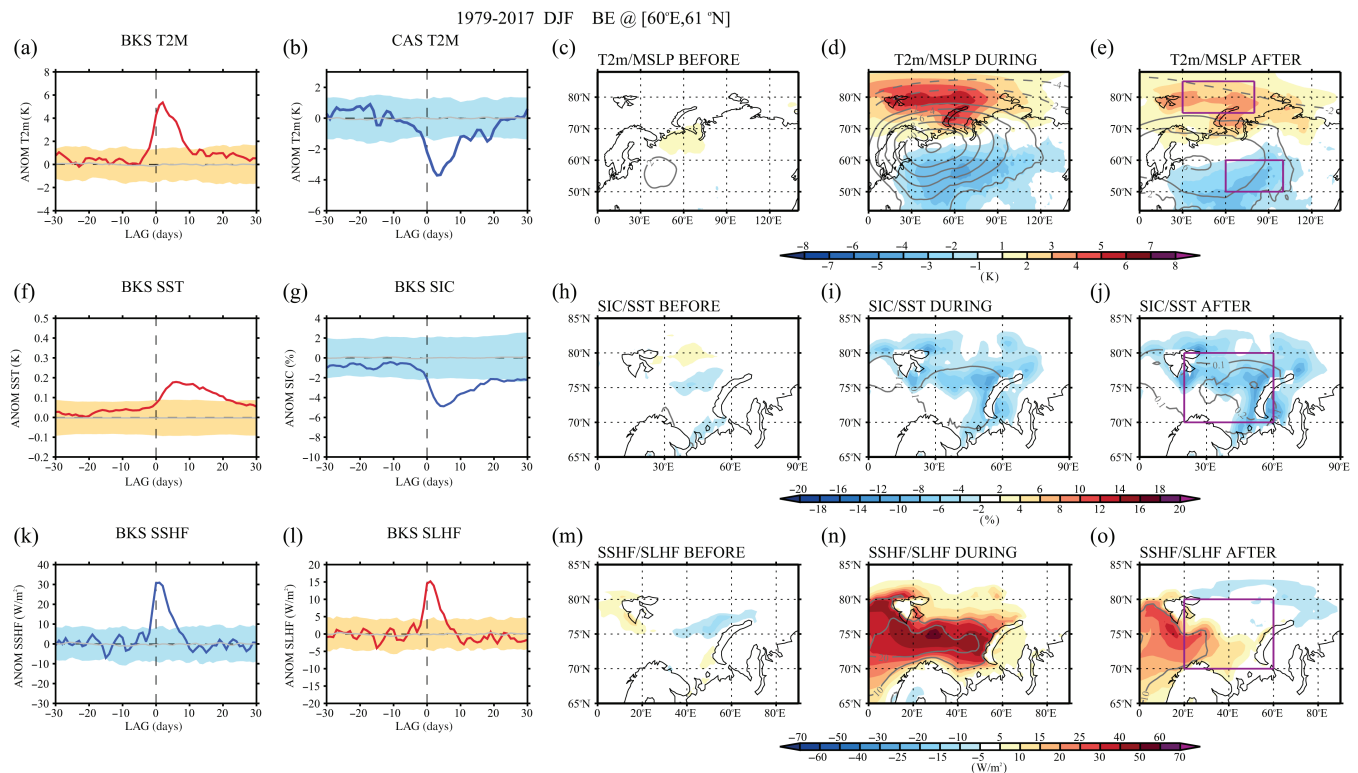


FIGURE 9 The same as Figure 8, but composites are shown for detrended time series of daily mean T2m, SIC, SST, SSHF and SLHF. The daily seasonal cycle has been first removed to produce anomalies, then the linear trend has been removed for each calendar day

The positive and negative impacts of UB on the DJF mean T2m over the BKS and CAS, respectively, are expected to depend primarily on the DJF mean UB frequency. Indeed, both impacts tend to be enhanced for winters with anomalously high UB activity (Figure 10c,d). Note also the statistically significant negative and positive correlations between the difference $T_{NOBE} - T_{ALL}$ for the BKS and CAS, respectively, and the DJF mean UB frequency. Thus, UB appears to significantly contribute to the interannual variability and temperature trend over CAS. A recent negative trend in the time series T_{NOBE} over CAS is only one third of its actual trend (Figure 10b). Although the cooling trend of T_{ALL} ($-1.6^{\circ}\text{C}/\text{decade}$) is statistically significant, exclusion of the UB days renders the trend non-robust. Given the high autocorrelation of the UB-induced temperature anomalies over CAS (Figure 8b), the impact of blocking may remain over the region even after its decay. Thus, the remaining blocking influence on CAS temperatures is inevitably included in the T_{NOBE} time series and its trend.

In contrast, over the BKS the trend is only slightly reduced in T_{NOBE} if compared to that in T_{ALL} (Figure 10a; both trends are statistically significant). Days without UB indeed tend to be cooler than the climatology over the BKS (grey line in Figure 10c). The background warming trend over the BKS is much stronger than the cooling

over CAS ($+4.3^{\circ}\text{C}$ and -1.6°C per decade, respectively; Figure 10a,b). Thus the exclusion of the UB days, which, on average, represent the minority among winter days, may not exert any substantial effect in reducing the BKS warming trend. Furthermore, despite the recent increase in UB activity, its average influence on the BKS warming has been steadily decreasing (Figures 10e and S8a,b). The meridional temperature gradient across the BKS has weakened from -0.55 to $-0.34^{\circ}\text{C}/^{\circ}\text{lat}$ between the earliest and latest ERA-Interim decades (Figure S8c,d). This change in the mean state can be attributed to the recent enhanced Arctic warming trend or to internal climate variability (Li *et al.*, 2018; Luo *et al.*, 2017b). It results in a weakening of the anomalous warm advection on the western flanks of the UB anticyclones. The weakening of the thermal advection and the temperature anomalies induced by blocking is expected to further intensify in the future due to the decreasing meridional temperature gradient (Masato *et al.*, 2014; Hoskins and Woollings, 2015). Unlike the BKS, the effect of UB on the CAS cooling trend has remained substantial and even slightly enhanced recently, although this trend is not statistically significant (Figure 10f). In conclusion, on interannual time-scales, UB appears to control the temperature variability over CAS and the BKS, although the trend over the BKS is dominated by processes related to Arctic amplification.

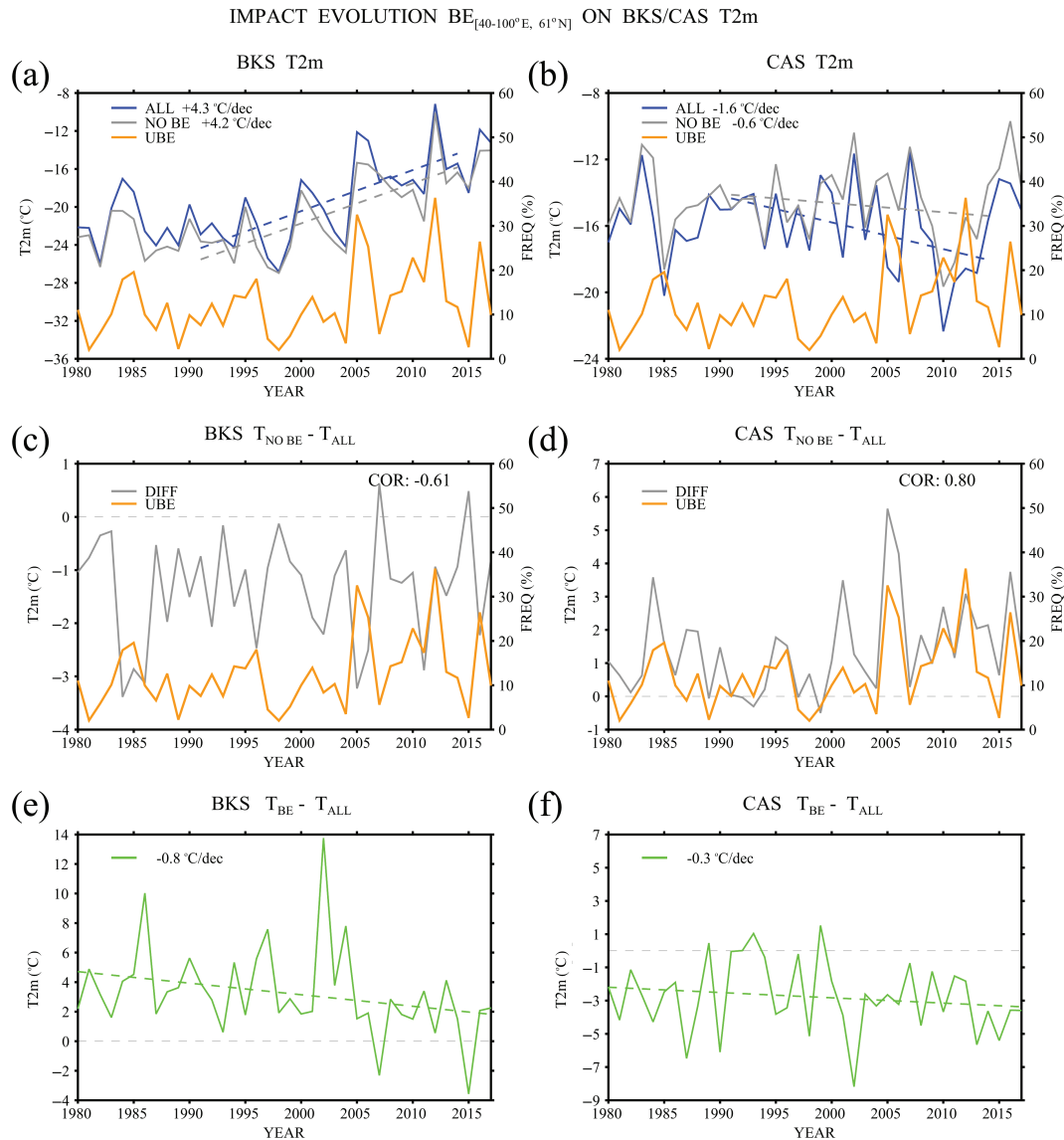


FIGURE 10 Interannual evolution of the DJF mean T2m area-averaged over (a) the BKS and (b) CAS, for all DJF days (T_{ALL} ; blue lines), for days without BE identified over the Ural sector (40–100°E, 61°N) (T_{NOBE} ; grey lines) and with the BE frequency averaged over the Ural sector (UBE frequency; orange lines). The difference $T_{NOBE} - T_{ALL}$ (grey) is shown for T2m averaged over (c) the BKS and (d) CAS, as well as UBE frequency (orange lines). The Pearson correlation coefficient between the two curves is also shown. The difference of the DJF mean T2m time series for DJF days when BE is identified over the Ural sector (T_{BE}) minus T_{ALL} time series is shown corresponding to (e) the BKS and (f) CAS T2m time series. The linear fit and the trend (°C per decade) during 1979–2017 are also shown. The BKS is defined as 40–90°E, 75–85°N and CAS as 60–100°E, 50–60°N. The statistical significance of linear trends and correlation coefficients is assessed with appropriate two-sided t-tests. Their values are given in bold text when found to be significant at the 95% level

7 | DISCUSSION AND CONCLUSIONS

Based on the analysis of non-detrended and detrended data for separate epochs of the ERA-Interim period, we have shown that the WACS pattern is a statistically robust pattern that represents an anti-correlation in area mean T2m between the BKS and CAS. UB is particularly efficient at inducing cooling over CAS and warming over the BKS, which markedly project onto the WACS pattern. Our

study is the first of its kind to use the PV- θ -based algorithm for the identification of blocking with a view to studying the UB-WACS link on a range of time-scales. The strong link that we have identified between the WACS pattern and UB activity is therefore an independent piece of evidence that supports previous studies (e.g., Luo *et al.*, 2016b, 2016a, 2019a; Chen *et al.*, 2018). In particular, by using a fully two-dimensional PV- θ blocking identification over Eurasia, we avoided any a priori regional assumptions to define UB. This approach has led to the novel result that

even within the Ural sector the latitude of blocking can be crucial. Indeed, blocking at higher latitudes is linked to an AO-like mode, which does not appear to be related to the WACS because it induces dipolar T2m anomalies that are shifted poleward compared to the WACS pattern.

We analysed daily fields to conclude that UB controls the pace of the WACS pattern on shorter time-scales, which is in line with the findings of Gong and Luo (2017) and Luo *et al.* (2016b, 2016a). The anticyclonic anomalies over the Ural sector induce anomalous warm advection over the BKS and cold surges over CAS, peaking 3–5 days after the UB onset. Under the warm advection over the BKS, SSTs increase over several days and then decrease slowly, while sea ice loss peaks several days after the blocking onset and then persists over more than 3 weeks. The fast build-up and decay of the anomalous downward surface heat fluxes, which follow the evolution of the T2m anomalies, suggests that sea ice variability on short time-scales is driven by the atmosphere. When examining the period prior to UB onset, the removal of the long-term trend in sea ice renders the observed sea ice deficit over the BKS non-robust, which may imply that the sea ice deficit does not have a direct influence on UB occurrence.

Winters with more frequent UB favour the emergence of the WACS signal in seasonal means. Thus, the interannual variability in T2m over the BKS and CAS is strongly linked to UB; during winters with high (low) UB activity, both BKS warming and CAS cooling are enhanced (weakened). The UB–WACS link is robust but weaker during the 1990s when the lowest UBE activity was observed (Figure 6). The role of other teleconnection patterns during this period should be investigated. The deeper warming over the Arctic following the late 1990s could be associated with a stronger UB–WACS link (Xu *et al.*, 2019). We have identified an upward trend in winter UB activity over recent decades that accounts for a cooling rate of at least 1°C per decade over CAS; the internal atmospheric variability associated with UB events emerges as the dominant process for inducing cooling trends over CAS. Although UB contributes to the warming over the BKS, the UB-induced warming does not account for most of the recent BKS warming trend, due to competing effects between the increasing UB days and the decreasing influence of individual UB events. Rather, it acts to enhance the strong background signal related to the Arctic amplification.

ACKNOWLEDGEMENTS

The results presented in this study were based on the ERA-Interim and COBE reanalysis data. Information on how to retrieve ERA-Interim reanalysis data from the European Centre for Medium-Range Weather Forecasts (ECMWF) can be found at the following link: [https://](https://www.ecmwf.int/en/forecasts/datasets/archive-datasets/reanalysis-datasets/era-interim)

www.ecmwf.int/en/forecasts/datasets/archive-datasets/reanalysis-datasets/era-interim. Information on how to retrieve the COBE reanalysis data can be found at https://ds.data.jma.go.jp/tcc/tcc/products/el_nino/cobesst/cobesst.html. The research that led to these results received funding from the German Federal Ministry of Education and Research (BMBF) through the CLIMPRE InterDec project (FKZ: 01LP1609A; E.T., D.M., J.B. and E.M.), the EU H2020 Blue-Action (GA 727852; E.M. and D.M.), the Japan Science and Technology Agency through the Belmont Forum CRA InterDec (H.N. and J.U.) and the Japanese Ministry of Education, Culture, Sports, Science and Technology through the ArCS Program (H.N. and J.U.). The authors wish to thank the editor for a very helpful review and are extremely appreciative of the comments of two anonymous reviewers. The constructive comments of Professor Klaus Fraedrich on an earlier version of the manuscript are also gratefully acknowledged.

ORCID

Evangelos Tyrlis  <https://orcid.org/0000-0002-0423-4926>

REFERENCES

- Barnes, E.A. (2013) Revisiting the evidence linking Arctic amplification to extreme weather in midlatitudes. *Geophysical Research Letters*, 40, 4734–4739. <https://doi.org/10.1002/grl.50880>
- Barnes, E.A., Dunn-Sigouin, E., Masato, G. and Woollings, T. (2014) Exploring recent trends in Northern Hemisphere blocking. *Geophysical Research Letters*, 41, 638–644. <https://doi.org/10.1002/2013GL058745>
- Barnes, E.A. and Screen, J.A. (2015) The impact of Arctic warming on the midlatitude jet-stream: can it? Has it? Will it?. *WIREs Climate Change*, 6, 277–286. <https://doi.org/10.1002/wcc.337>
- Berrisford, P., Hoskins, B.J. and Tyrlis, E. (2007) Blocking and Rossby wave breaking on the dynamical tropopause in the Southern Hemisphere. *Journal of the Atmospheric Sciences*, 64, 2881–2898. <https://doi.org/10.1175/JAS3984.1>
- Chen, X., Luo, D., Feldstein, S.B. and Lee, S. (2018) Impact of winter Ural blocking on Arctic sea ice: short-time variability. *Journal of Climate*, 31, 2267–2282. <https://doi.org/10.1175/JCLI-D-17-0194.1>
- Cheung, H.H.N. and Zhou, W. (2015) Implications of Ural blocking for East Asian winter climate in CMIP5 GCMs. Part II: projection and uncertainty in future climate conditions. *Journal of Climate*, 28, 2217–2233. <https://doi.org/10.1175/JCLI-D-14-00309.1>
- Cohen, J., Screen, J.A., Furtado, J.C., Mathew, B., Whittleston, D., Coumou, D., Francis, J., Dethloff, K., Entekhabi, D., Overland, J. and Jones, J. (2014) Recent Arctic amplification and extreme mid-latitude weather. *Nature Geosciences*, 7, 627–637. <https://doi.org/10.1038/NNGEO2234>
- Davini, P., Cagnazzo, C., Gualdi, S. and Navarra, A. (2012) Bidimensional diagnostics, variability, and trends of Northern Hemisphere blocking. *Journal of Climate*, 25, 6496–6509. <https://doi.org/10.1175/JCLI-D-12-00032.1>
- Dee, D.P., Uppala, S.M., Simmons, A.J., Berrisford, P., Poli, P., Kobayashi, S., Andrae, U., Balmaseda, M.A., Balsamo, G., Bauer,

- P., Bechtold, P., Beljaars, A.C.M., van de Berg, L., Bidlot, J., Bormann, N., Delsol, C., Dragani, R., Fuentes, M., Geer, A.J., Haimberger, L., Healy, S.B., Hersbach, H., Hólm, E.V., Isaksen, I., Kållberg, P., Köhler, M., Matricardi, M., McNally, A.P., Monge-Sanz, B.M., Morcrette, J.-J., Park, B.-K., Peubey, C., de Rosnay, P., Tavolato, C., Thépaut, J.-N. and Vitart, F. (2011) The ERA-Interim reanalysis: configuration and performance of the data assimilation system. *Quarterly Journal of the Royal Meteorological Society*, 137, 553–597. <https://doi.org/10.1002/qj.828>
- Deser, C., Guo, R. and Lehner, F. (2017) The relative contributions of tropical Pacific sea surface temperatures and atmospheric internal variability to the recent global warming hiatus. *Geophysical Research Letters*, 44, 7945–7954. <https://doi.org/10.1002/2017GL074273>
- Fischer, E.M. and Knutti, R. (2014) Impacts: heated debate on cold weather. *Nature Climate Change*, 4, 537–538. <https://doi.org/10.1038/nclimate2286>
- Francis, J.A. and Vavrus, S.J. (2012) Evidence linking Arctic amplification to extreme weather in mid-latitudes. *Geophysical Research Letters*, 39, L06801. <https://doi.org/10.1029/2012GL051000>
- Francis, J.A. and Vavrus, S.J. (2015) Evidence for a wavier jet stream in response to rapid Arctic warming. *Environmental Research Letters*, 10, 014005. <https://doi.org/10.1088/1748-9326/10/1/014005>
- Gong, T. and Luo, D. (2017) Ural blocking as an amplifier of the Arctic sea ice decline in winter. *Journal of Climate*, 30, 2639–2654. <https://doi.org/10.1175/JCLI-D-16-0548.1>
- Hirahara, S., Ishii, M. and Fukuda, Y. (2014) Centennial-scale sea surface temperature analysis and its uncertainty. *Journal of Climate*, 27, 57–75. <https://doi.org/10.1175/JCLI-D-12-00837.1>
- Honda, M., Inoue, J. and Yamane, S. (2009) Influence of low Arctic sea-ice minima on anomalously cold Eurasian winters. *Geophysical Research Letters*, 36, L08707. <https://doi.org/10.1029/2008GL037079>
- Horton, D.E., Johnson, N.C., Singh, D., Swain, D.L., Rajaratnam, B. and Diffenbaugh, N.S. (2015) Contribution of changes in atmospheric circulation patterns to extreme temperature trends. *Nature*, 522, 465–469. <https://doi.org/10.1038/nature14550>
- Hoshi, K., Ukita, J., Honda, M., Iwamoto, K., Nakamura, T., Yamazaki, K., Dethloff, K., Jaiser, R. and Handorf, D. (2017) Poleward eddy heat flux anomalies associated with recent Arctic sea ice loss. *Geophysical Research Letters*, 44, 446–454. <https://doi.org/10.1002/2016GL071893>
- Hoskins, B.J., McIntyre, M.E. and Robertson, A.W. (1985) On the use and significance of isentropic potential vorticity maps. *Quarterly Journal of the Royal Meteorological Society*, 111, 877–946. <https://doi.org/10.1002/qj.49711147002>
- Hoskins, B.J. and Woollings, T. (2015) Persistent extratropical regimes and climate extremes. *Current Climate Change Reports*, 1, 115–124. <https://doi.org/10.1007/s40641-015-0020-8>
- Inoue, J., Hori, M.E. and Takaya, K. (2012) The role of Barents sea ice in the wintertime cyclone track and emergence of a warm-Arctic cold-Siberian anomaly. *Journal of Climate*, 25, 2561–2568. <https://doi.org/10.1175/JCLI-D-11-00449.1>
- Kretschmer, M., Coumou, D., Donges, J.F. and Runge, J. (2016) Using causal effect networks to analyze different Arctic drivers of mid-latitude winter circulation. *Journal of Climate*, 29, 4069–4081. <https://doi.org/10.1175/JCLI-D-15-0654.1>
- Kug, J.-S., Jeong, J.-H., Jang, Y.-S., Kim, B.-M., Folland, C.K., Min, S.-K. and Son, S.-W. (2015) Two distinct influences of Arctic warming on cold winters over North America and East Asia. *Nature Geosciences*, 8, 759–762. <https://doi.org/10.1038/ngeo2517>
- Lee, S., Gong, T., Feldstein, S.B., Screen, J.A. and Simmonds, I. (2017) Revisiting the cause of the 1989–2009 Arctic surface warming using the surface energy budget: downward infrared radiation dominates the surface fluxes. *Geophysical Research Letters*, 44, 10654–10661. <https://doi.org/10.1002/2017GL075375>
- Li, C., Stevens, B. and Marotzke, J. (2015) Eurasian winter cooling in the warming hiatus of 1998–2012. *Geophysical Research Letters*, 42, 8131–8139. <https://doi.org/10.1002/2015GL065327>
- Li, F., Orsolini, Y.J., Wang, H., Gao, Y. and He, S. (2018) Atlantic multidecadal oscillation modulates the impacts of Arctic sea ice decline. *Geophysical Research Letters*, 45, 2497–2506. <https://doi.org/10.1002/2017GL076210>
- Luo, B., Luo, D., Wu, L., Zhong, L. and Simmonds, I. (2017a) Atmospheric circulation patterns which promote Arctic sea ice decline. *Environmental Research Letters*, 12, 054017. <https://doi.org/10.1088/1748-9326/aa69d0>
- Luo, B., Wu, L., Luo, D., Dai, A. and Simmonds, I. (2019a) The winter midlatitude-Arctic interaction: effects of North Atlantic SST and high-latitude blocking on Arctic sea ice and Eurasian cooling. *Climate Dynamics*, 52, 2981–3004. <https://doi.org/10.1007/s00382-018-4301-5>
- Luo, D., Chen, X., Dai, A. and Simmonds, I. (2018) Changes in atmospheric blocking circulations linked with winter Arctic warming: a new perspective. *Journal of Climate*, 31, 7661–7678. <https://doi.org/10.1175/JCLI-D-18-0040.1>
- Luo, D., Chen, X., Overland, I., Simmonds, I., Wu, Y. and Zhang, P. (2019b) Weakened potential vorticity barrier linked to recent winter Arctic sea ice loss and midlatitude cold extremes. *Journal of Climate*, 32, 4235–4261. <https://doi.org/10.1175/JCLI-D-18-0449.1>
- Luo, D., Chen, Y., Dai, A., Mu, M., Zhang, R. and Simmonds, I. (2017b) Winter Eurasian cooling linked with the Atlantic multidecadal oscillation. *Environmental Research Letters*, 12, 125002. <https://doi.org/10.1088/1748-9326/aa8de8>
- Luo, D., Xiao, Y., Diao, Y., Dai, A., Franzke, C.L.E. and Simmonds, I. (2016a) Impact of Ural blocking on winter warm Arctic–cold Eurasian anomalies. Part II: the link to the North Atlantic Oscillation. *Journal of Climate*, 29, 3949–3971. <https://doi.org/10.1175/JCLI-D-15-0612.1>
- Luo, D., Xiao, Y., Yao, Y., Dai, A., Simmonds, I. and Franzke, C.L.E. (2016b) Impact of Ural blocking on winter warm Arctic–cold Eurasian anomalies. Part I: blocking induced amplification. *Journal of Climate*, 29, 3925–3947. <https://doi.org/10.1175/JCLI-D-15-0611.1>
- Luo, D., Yao, Y., Dai, A., Simmonds, I. and Zhong, L. (2017c) Increased quasi stationarity and persistence of winter Ural blocking and Eurasian extreme cold events in response to Arctic warming. Part II: theoretical explanation. *Journal of Climate*, 30, 3569–3587. <https://doi.org/10.1175/JCLI-D-16-0262.1>
- Luo, D., Zhang, W., Zhong, L., Simmonds, I. and Dai, A. (2019c) A nonlinear theory of atmospheric blocking: a potential vorticity gradient view. *Journal of the Atmospheric Sciences*, 76, 2399–2427. <https://doi.org/10.1175/JAS-D-18-0324.1>
- Masato, G., Woollings, T.J. and Hoskins, B.J. (2014) Structure and impact of atmospheric blocking over the Euro-Atlantic region in present day and future simulations. *Geophysical Research Letters*, 41, 1051–1058. <https://doi.org/10.1002/2013GL058570>

- Mori, M., Kosaka, Y., Watanabe, M., Nakamura, H. and Kimoto, M. (2019a) A reconciled estimate of the influence of Arctic sea-ice loss on recent Eurasian cooling. *Nature Climate Change*, 9, 123–129. <https://doi.org/10.1038/s41558-018-0379-3>
- Mori, M., Kosaka, Y., Watanabe, M., Taguchi, B., Nakamura, H. and Kimoto, M. (2019b) Reply to: Is sea-ice-driven Eurasian cooling too weak in models?. *Nature Climate Change*, 9, 937–939. <https://doi.org/10.1038/s41558-019-0636-0>
- Mori, M., Watanabe, M., Shiogama, H., Inoue, J. and Kimoto, M. (2014) Robust Arctic sea-ice influence on the frequent Eurasian cold winters in past decades. *Nature Geosciences*, 7, 869–873. <https://doi.org/10.1038/ngeo2277>
- Nakamura, T., Yamazaki, K., Iwamoto, K., Honda, M., Miyoshi, Y., Ogawa, Y., Tomikawa, Y. and Ukita, J. (2016) The stratospheric pathway for Arctic impacts on midlatitude climate. *Geophysical Research Letters*, 43, 3494–3501. <https://doi.org/10.1002/2016GL068330>
- Orsolini, Y.J., Senan, R., Benestad, R.E. and Melsom, A. (2012) Autumn atmospheric response to the 2007 low Arctic sea ice extent in coupled ocean-atmosphere hindcasts. *Climate Dynamics*, 38, 2437–2448. <https://doi.org/10.1007/s00382-011-1169-z>
- Peings, Y. (2019) Ural blocking as a driver of early-winter stratospheric warmings. *Geophysical Research Letters*, 46, 5460–5468. <https://doi.org/10.1029/2019GL082097>
- Pelly, J. and Hoskins, B.J. (2003) A new perspective on blocking. *Journal of the Atmospheric Sciences*, 60, 743–755. [https://doi.org/10.1175/1520-0469\(2003\)060<0743:ANPOB>2.0.CO;2](https://doi.org/10.1175/1520-0469(2003)060<0743:ANPOB>2.0.CO;2)
- Petoukhov, V. and Semenov, V.A. (2010) A link between reduced Barents-Kara sea ice and cold winter extremes over northern continents. *Journal of Geophysical Research*, 115, D21111. <https://doi.org/10.1029/2009JD013568>
- Screen, J.A. and Blackport, R. (2019) Is sea-ice-driven Eurasian cooling too weak in models?. *Nature Climate Change*, 9, 934–936. <https://doi.org/10.1038/s41558-019-0635-1>
- Screen, J.A., Simmonds, I., Deser, C. and Tomas, R. (2013) The atmospheric response to three decades of observed Arctic sea ice loss. *Journal of Climate*, 26, 1230–1248. <https://doi.org/10.1175/JCLI-D-12-00063.1>
- Sorokina, S.A., Li, C., Wettstein, J.S. and Kvamstø, N.G. (2016) Observed atmospheric coupling between Barents sea ice and the warm-Arctic cold-Siberian anomaly pattern. *Journal of Climate*, 29, 495–511. <https://doi.org/10.1175/JCLI-D-15-0046.1>
- Sun, L., Perlwitz, J. and Hoerling, M. (2016) What caused the recent “Warm Arctic, Cold Continents” trend pattern in winter temperatures?. *Geophysical Research Letters*, 43, 5345–5352. <https://doi.org/10.1002/2016GL069024>
- Sung, M.-K., Kim, S.-H., Kim, B.-M. and Choi, Y.-S. (2018) Interdecadal variability of the warm Arctic and cold Eurasia pattern and its North Atlantic origin. *Journal of Climate*, 31, 5793–5809. <https://doi.org/10.1175/JCLI-D-17-0562.1>
- Takaya, K. and Nakamura, H. (2005) Mechanisms of intraseasonal amplification of the cold Siberian high. *Journal of the Atmospheric Sciences*, 62, 4423–4440. <https://doi.org/10.1175/JAS3629.1>
- Tibaldi, S. and Molteni, F. (1990) On the operational predictability of blocking. *Tellus A*, 42, 343–365. <https://doi.org/10.1034/j.1600-0870.1990.t01-2-00003.x>
- Tyrlis, E. and Hoskins, B.J. (2008) Aspects of a Northern Hemisphere atmospheric blocking climatology. *Journal of the Atmospheric Sciences*, 65, 1638–1652. <https://doi.org/10.1175/2007JAS2337.1>
- Tyrlis, E., Manzini, E., Bader, J., Ukita, J., Nakamura, H. and Matei, D. (2019) Ural blocking driving extreme Arctic sea ice loss, Cold Eurasia, and stratospheric vortex weakening in autumn and early winter 2016–2017. *Journal of Geophysical Research*, 124, 11313–11329. <https://doi.org/10.1029/2019JD031085>
- Tyrlis, E., Tymvios, F.S., Giannakopoulos, C. and Lelieveld, J. (2015) The role of blocking in the summer 2014 collapse of Etesians over the Eastern Mediterranean. *Journal of Geophysical Research*, 120, 6777–6792. <https://doi.org/10.1002/2015JD023543>
- Wang, L. and Chen, W. (2014) The East Asian winter monsoon: re-amplification in the mid-2000s. *Chinese Science Bulletin*, 59, 430–436. <https://doi.org/10.1007/s11434-013-0029-0>
- Wang, L., Huang, R., Gu, L., Chen, W. and Kang, L. (2009) Interdecadal variations of the East Asian Winter Monsoon and their association with quasi-stationary planetary wave activity. *Journal of Climate*, 22, 4860–4872. <https://doi.org/10.1175/2009JCLI2973.1>
- Woods, C. and Caballero, R. (2013) The role of moist intrusions in winter Arctic warming and sea ice decline. *Journal of Climate*, 29, 4473–4485. <https://doi.org/10.1175/JCLI-D-15-0773.1>
- Woods, C., Caballero, R. and Svensson, G. (2013) Large-scale circulation associated with moisture intrusions into the Arctic during winter. *Geophysical Research Letters*, 40, 4717–4121. <https://doi.org/10.1002/grl.50912>
- Woollings, T.J., Hoskins, B.J., Blackburn, P. and Berrisford, P. (2008) A new Rossby wave-breaking interpretation of the North Atlantic Oscillation. *Journal of the Atmospheric Sciences*, 65, 609–626. <https://doi.org/10.1175/2007JAS2347.1>
- Xu, X., He, S., Gao, Y., Furevik, T., Wang, H., Li, F. and Ogawa, F. (2019) Strengthened linkage between midlatitudes and Arctic in boreal winter. *Climate Dynamics*, 53, 3971–3983. <https://doi.org/10.1007/s00382-019-04764-7>
- Yao, Y., Luo, D., Dai, A. and Simmonds, I. (2017) Increased quasi stationarity and persistence of winter Ural blocking and Eurasian extreme cold events in response to Arctic warming. Part I: insights from observational analyses. *Journal of Climate*, 30, 3549–3568. <https://doi.org/10.1175/JCLI-D-16-0261.1>
- Ye, K., Jung, T. and Semmler, T. (2018) The influences of the Arctic troposphere on the midlatitude climate variability and the recent Eurasian cooling. *Journal of Geophysical Research*, 123, 10162–10184. <https://doi.org/10.1029/2018JD028980>
- Zhang, X., Lu, C. and Guan, Z. (2012) Weakened cyclones, intensified anticyclones and recent cold winter weather events in Eurasia. *Environmental Research Letters*, 7, 044044. <https://doi.org/10.1088/1748-9326/7/4/044044>

How to cite this article: Tyrlis E, Bader J, Manzini E, Ukita J, Nakamura H, Matei D. On the role of Ural Blocking in driving the Warm Arctic–Cold Siberia pattern. *Q J R Meteorol Soc.* 2020;146:2138–2153. <https://doi.org/10.1002/qj.3784>